ARTICLE NO. 78-18R

J80-226

Measurements of Unsteady Vortex Flowfields

20009

F. K. Owen*
Palo Alto, Calif.
and
D. A. Johnson†
NASA Ames Research Center, Moffett Field, Calif.

A combined surface hot film and laser velocimeter measurement technique has been developed for the study of time-dependent turbulent flows. Data obtained in a compressible cylinder wake ($M_\infty = 0.6$) are presented, and its structure in both the Eulerian and Lagrangian frames is discussed. Turbulence data obtained by conventional and phase averaging of the velocity fluctuations provide details of the small- and large-scale contributions to the total turbulent field.

Introduction

CONSIDERABLE attention and effort have been directed to the area of conditional sampling as a means of revealing flow features which appear intermittently rather than continuously, yet still have an important influence on flow structure and development. However, until recently, these efforts were all restricted to experiments in which the flowfield sensor had a continuous output which could be used to generate the criteria for the conditional averages; so that measurements were of necessity restricted to unidirectional shear flows in which, for example, standard hot-wire anemometry techniques could be used. Whole classes of flows, namely recirculating and unsteady wake flows, were therefore neglected. In these flows, it is extremely difficult to generate reliable analog or digital outputs with conventional flowfield instrumentation, since these flows are extremely sensitive to probe interference.

Unfortunately, laser velocimeter data alone are usually difficult to sample conditionally since in most cases the data rates are insufficient to generate real-time information from which the sampling criteria can be determined. A technique close to conditional sampling can be used to generate ensemble averages at given phase angles in turbulent flows superimposed on periodic motions, such as those in reciprocating machinery or helicopter wakes, for example. In these cases, the sampling condition can be derived from a periodic timing signal. However, in the case of aerodynamic oscillations whose period is not exactly constant, i.e., the vortex sheet behind a bluff body, the sampling condition must be derived from the flow itself.

Because of these experimental difficulties, few measurements are available of time-dependent wake flows. Although recent mean measurements using laser streak velocimetry have been made,[1] this technique cannot be used to determine turbulent structure nor be applied directly to high-speed flows.

A comparison of the wake structure of a stationary and oscillating D-shaped cylinder using hot-wire anemometer conditional averaging has recently been reported by Davies.[2] However, data were not obtained closer than 8 cylinder diameters from the body. Closer to the body, directional ambiguity will affect the hot-wire velocity and turbulence measurements. A flying hot-wire technique has been used by Cantwell[3] to make measurements in highly turbulent flows involving large excursions in flow direction and has been used to study the near wake of a circular cylinder at low speed. But, as pointed out in the conclusions of Ref. 3, the technique at that time was somewhat complicated and unwieldy, and the issue concerning the disturbance of the flowfield by the rotating arms remained largely unresolved. In addition, it is doubtful whether rotation speeds could be used to provide sufficient zero offset in high-speed flows and to overcome hot-wire data interpretation problems in the transonic regime.

Thus, the purpose of this paper is to describe a combined nonintrusive surface thin film gage and laser velocimeter technique which can be used in both low- and high-speed flows to obtain new information on the mean and turbulent structure of time-dependent flowfields. New information obtained by this sampling technique of the time-dependent mean flowfield behind a circular cylinder and of the large- and small-scale turbulent structure of the wake is presented. Comparisons are also made with the near-wake data of Ref. 3.

Experimental Details

The experiments were conducted in the Ames 2×2 ft wind tunnel on a circular cylinder of aspect ratio 24:1, in crossflow at a Reynolds number of 167,000 in the transonic regime ($M_\infty = 0.6$). The cylinder was instrumented with constant temperature surface hot film gages of the type used in Ref. 4. The dynamic gage response (>60 kHz with negligible phase distortion) was sufficient to determine the time history of the vortex shedding.

These gage outputs were used to trigger a single-component frequency offset forward scatter laser velocimeter which generated conditionally sampled axial and vertical velocity distributions in the unsteady vortex flow behind the cylinder. In this way, the vortex structures and strengths were determined.

A schematic representation of the instrumentation is shown in Fig. 1. The procedure of operation is as follows: The surface gage output is used to initiate a pulse which can be varied in length and time delay from when the surface gage achieves a present threshold level of given slope. This pulse then actuates the AND gate. Thus, only Doppler signals arriving during the pulse are processed. By proper choice of trigger level, time delay, and pulse length, a suitable data window can be achieved so that the unsteady flow can be frozen and the vortex field determined. However, in the actual wind tunnel tests, records of both the surface hot film and laser velocimeter outputs were recorded on tape for later analysis. This procedure greatly decreased the wind tunnel test time requirement.

Presented as Paper 78-18 at the AIAA 16th Aerospace Sciences Meeting, Huntsville, Ala., Jan. 16-18, 1978; submitted April 3, 1978; revision received Feb. 22, 1980. This paper is declared a work of the U.S. Government and therefore is in the public domain.

Index category: Nonsteady Aerodynamics.

*Consultant, P.O. Box 1697. Member AIAA.

†Research Scientist. Member AIAA.

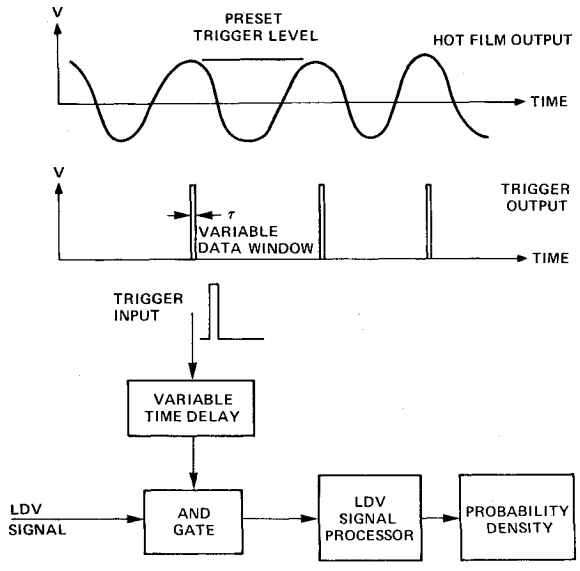

Fig. 1 Schematic of the conditional sampling electronics.

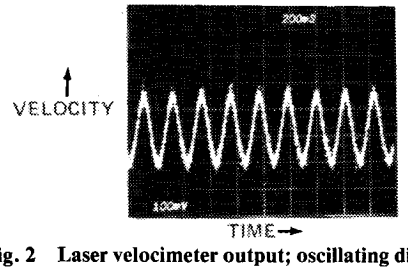

Fig. 2 Laser velocimeter output; oscillating disk.

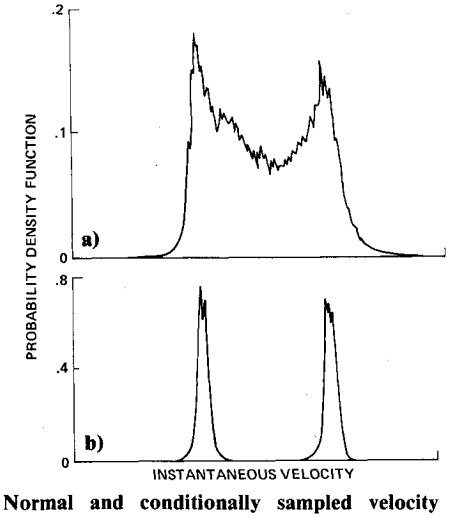

Fig. 3 Normal and conditionally sampled velocity probability density distributions.

Discussion

To illustrate the technique, results obtained from a continuously variable velocity source are shown in Figs. 2 and 3. In this case, the velocity of an oscillating, rotating disk was measured, and the trigger pulses were generated from a fixed location on the wheel itself. The uninterrupted laser velocimeter analog output is shown in Fig. 2. These measurements show the nature of the instantaneous velocity variations. Without conditional sampling, the probability density shown in Fig. 3a is determined. This distribution, which closely resembles the shape expected from a sinusoidal input, can then be used to determine the time-averaged mean and rms velocities in the usual way. Examples of conditionally sampled data are shown in Fig. 3b, where it can be seen that

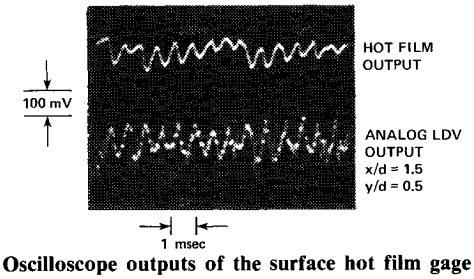

Fig. 4 Oscilloscope outputs of the surface hot film gage and laser anemometer.

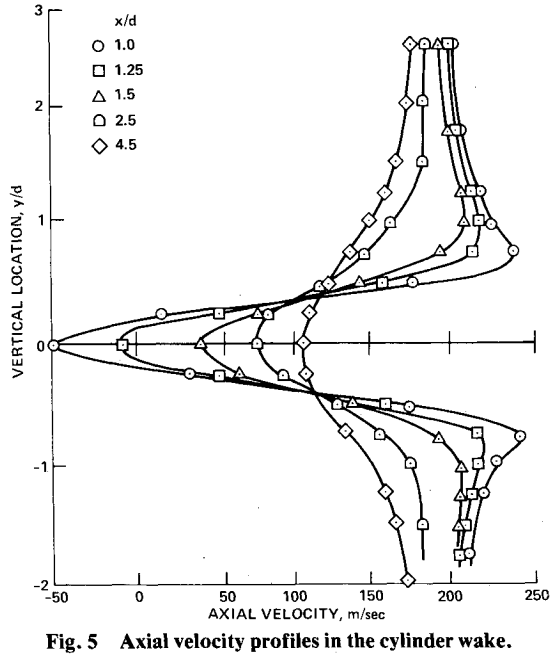

Fig. 5 Axial velocity profiles in the cylinder wake.

with suitable choice of data window width and time delay, sharp peaks corresponding to the two extreme velocities can be determined.

In the wind tunnel, a surface thin film gage was used to generate the sampling condition in the cylinder vortex tests, since gage oscillations are related to vortex shedding in the wake and, thus, give an indication of their passage downstream through the plane of the LDV measuring station. The principle of the conditional sampling technique was to use the surface gage output to provide a reference phase angle to which the wake velocity could be related. It is important to realize that the same average could not be obtained by bandpass filtering about the shedding frequency, since this would exclude any harmonic velocity fluctuations but would include the unwanted part of the small-scale turbulent spectrum within the filtering band. Neither is the sampling periodic for it allows for irregularities in the shedding process. Oscilloscope outputs of a surface hot film gage and the analog output of the velocimeter, obtained at a Reynolds number of 2 million/ft and a Mach number of 0.85, are shown in Fig. 4. After suitable signal conditioning, such clearly defined Strouhal frequencies provided adequate trigger level resolution for conditional sampling of the laser velocimeter data. Since, with forward scatter, velocimeter data rates in excess of 50,000/s with seeding were achieved, this combined bluff body surface-flowfield sampling technique provided a powerful method of determining the time-dependent cylinder wake structure.

Results

Mean Flowfield

Time-averaged axial velocity profiles obtained in the cylinder wake are presented in Fig. 5. These data indicate the

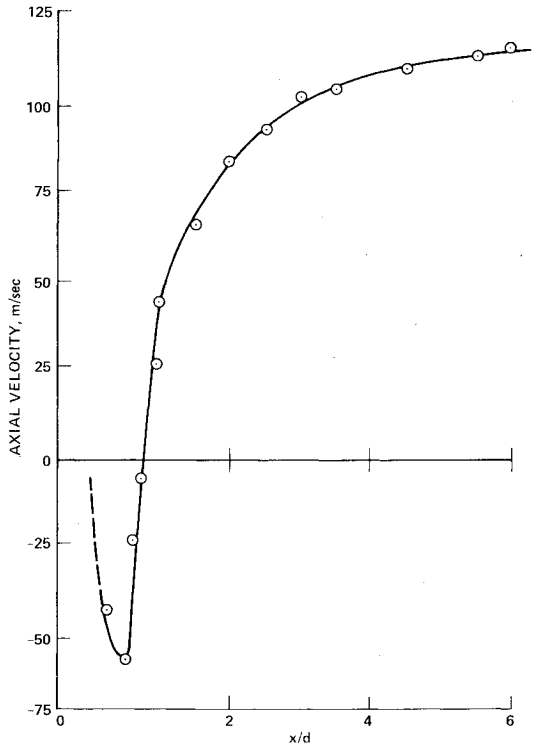

Fig. 6 Wake centerline velocity profile.

extent of the mean flow separation and the decay of the wake defect velocity. They also show regions of extremely high mean shear and significant velocity overshoots $(u/u_\infty)_{max} \simeq 1.25$ in the profiles closest to the separation points. However, both of these features decay rapidly, an indication of extremely energetic turbulent motions in the wake. The mean axial velocity profile obtained along the wake centerline $(y/d=0)$ is shown in Fig. 6, where it can be seen that the mean wake closure occurs 1.3 diameters behind the cylinder centerline. This extent of mean flow reversal is relatively small and compares very favorably with Cantwell's value of 1.1. A plot of the wake defect velocity (Fig. 7a) clearly shows that the wake can be divided into two distinct zones. Assuming that the region of most rapid wake defect decay represents the extent of the vortex formation region, that is, the region of highest entrainment and mixing, it can be seen that instantaneous vortex formation can still take place well downstream of the mean closure point in the wake.

Although the qualitative trends are similar, large quantiative differences between the present measurements and those of Ref. 3 are apparent. A comparison (Fig. 7b) of the data with Schlichting's far-wake experiments and the predictions of Ref. 5 show that the present near-wake measurements are in excellent agreement with previous observations.

Another interesting feature of the axial velocity measurements is their apparent similarity in the near-wake region (Fig. 8) when normalized by the local maximum values. The agreement with Schlichting's far-wake correlation is extremely good.

Mean vertical velocity measurements were also obtained throughout the wake. An example obtained at $x/d=1.5$ is shown in Fig. 9. These data show the extent of mean fluid entrainment into the wake, the maximum crossflow velocities toward the wake centerline being approximately 30% of the freestream velocity. Closer to the cylinder, $x/d=0.75$ mean fluid motion away from the wake centerline approached 50% of the freestream velocity.

Point measurements of these mean axial and vertical velocities throughout the wake have been used to construct a velocity vector plot of the mean flowfield which is shown in

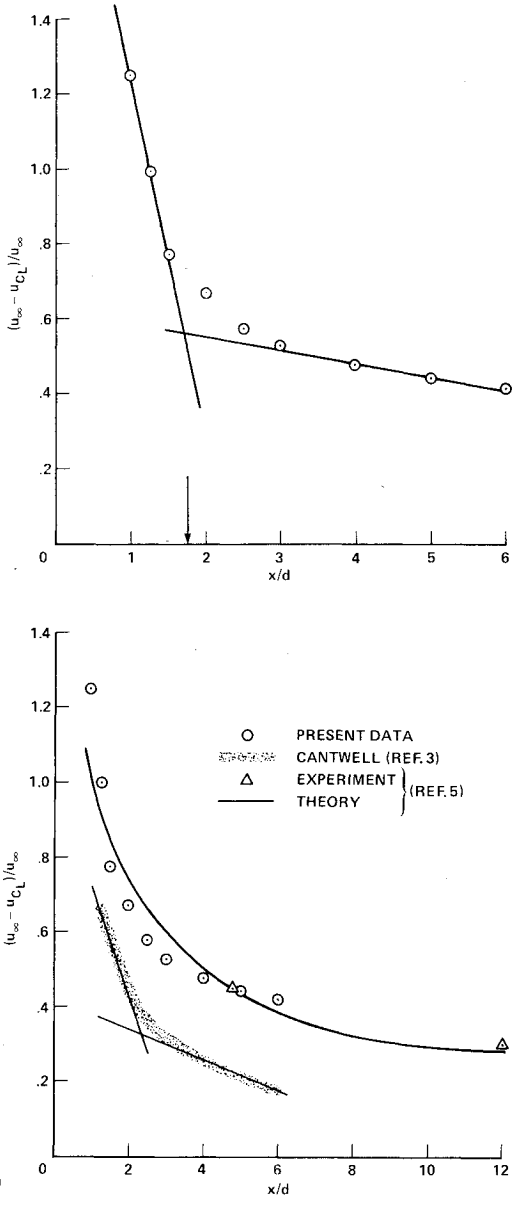

Fig. 7 Wake velocity defect; a) present measurements, b) comparison of near-wake measurements and theory with an assumed drag coefficient of 1.2.

Fig. 10. Since the length of the velocity vectors outside the wake correspond to the freestream velocity (200 m/s), this figure gives quantitative information on the global flowfield. Curves have been drawn through the tips of vectors at two axial locations to indicate the velocity defect in the wake.

Time-Dependent (Constant Phase-Averaged) Velocity Measurements

Now let us turn our attention to the measurements obtained at constant phase during the shedding cylce. Since the flow repeats itself periodically, we can sample the velocity when the shedding vortices are at some given position in the flow. One cycle later we can sample again, and thus, over many cycles, build up an ensemble average at constant phase. These velocities represent the regular- and small-scale random behavior of the flow at a fixed point in the flowfield with the vortices frozen in some average position.

To illustrate some of the measurements, data taken in the wake 2.5 diameters downstream of the cylinder $(x/d=2.5)$ are shown in Fig. 11. On the axis, positive and negative vertical velocities are equally probable. Thus, conventional averaging would give a time-averaged velocity close to zero and a large rms velocity fluctuation level which is, of course, due to

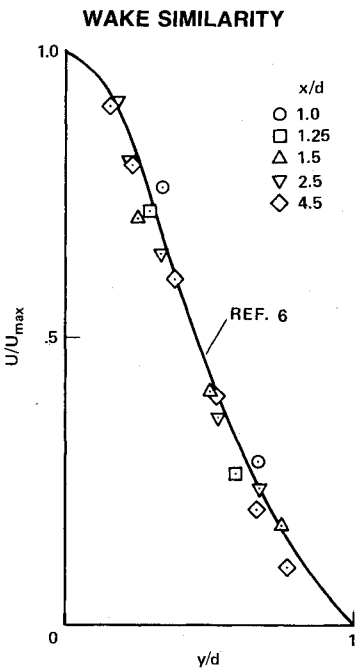

Fig. 8 Normalized axial velocity distributions in the wake.

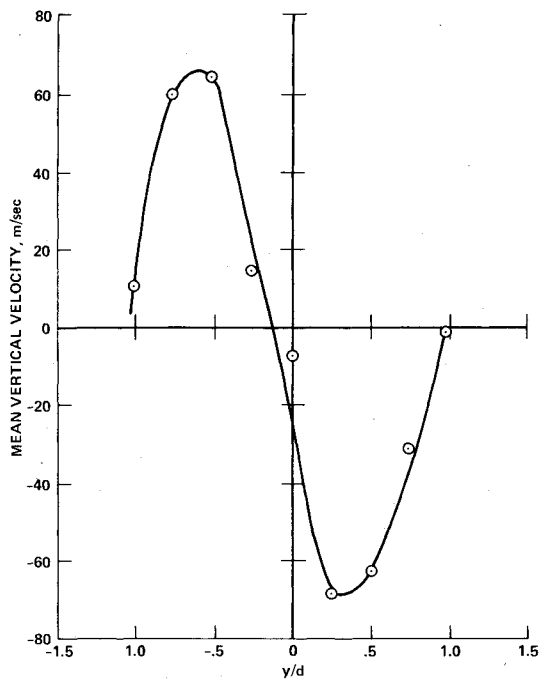

Fig. 9 Vertical velocity profile $x/d = 1.5$.

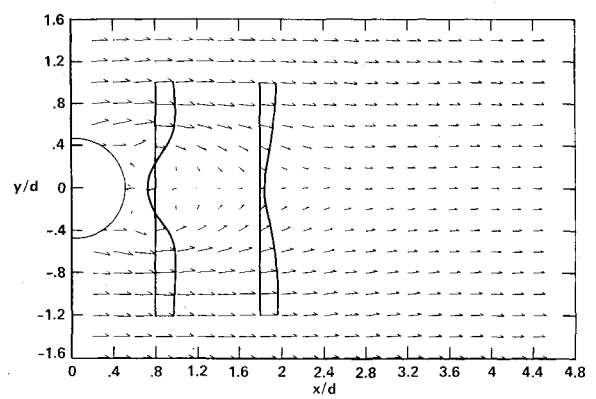

Fig. 10 Mean velocity vectors.

instantaneous changes in induced mean flow velocity caused by alternate vortex shedding. Above the centerline ($y/d = 0.5$), the probability density function is still bimodal, although negative vertical velocities predominate, as here the local flow is determined more by vortex shedding from the upper surface. In this case, conventional averaging would indicate a small negative vertical velocity and a large rms. Below the axis ($y/d = -0.5$), positive vertical velocities induced by vortex shedding from the lower surface are more likely, but again, conventional averaging would lose the true nature of the time-dependent local flowfield. However, outside the wake (e.g., $y/d = -1.75$), where single-peaked probability distributions occur, time-averaged data are now sufficient to determine the local flow features.

To determine the time-dependent nature of the wake, the bimodal velocity distributions must be conditionally sampled, as described previously. Typical results are shown in Fig. 12 for velocity samples taken at peak and minimum thin film gage output, that is, 180-deg phase shift in the shedding cycle. However, as can be seen in Fig. 12, it was not possible to eliminate velocity occurrences from different phases completely, principally because of the random fluctuations superimposed on the large-scale vortices and because there must be some dispersion, that is, all shed vortices were not exactly the same. These effects were reduced to a large extent by considering only the shaded contribution to the velocity probability density when calculating the local time-dependent velocities. Data obtained throughout the shedding cycle are shown in Fig. 13, where it can be seen that the conditionally sampled vertical velocity variations are approximately sinusoidal, their period corresponding to that of the Strouhal shedding frequency (approximately 1400 Hz). Indeed, surface gage and laser velocimeter power spectral densities, which will be presented later in the paper, will confirm this.

These data can then be used to construct time-dependent velocity vector plots of the cylinder wake. Such plots (Figs. 14a and 14b) show the flowfield 180 deg apart, corresponding to vortex shedding from the upper and lower surface of the cylinder. In this frame of reference which is at rest with the cylinder, i.e., the Eulerian frame, the wake flow has a wavy character with a wave length of approximately 3.5 cylinder diameters with a wave speed, based on Strouhal shedding frequency, of about 125 m/s.

Vortex convection velocity measurements have also been obtained more directly by cross correlation of the surface hot film and laser velocimeter outputs. For these correlation measurements ($x = 1.5$, $y = 1.0$), the wind tunnel was seeded with 0.7-μm particles at concentrations which gave data rates of approximately 50 kHz. Such a data rate is adequate to resolve the 1.4 kHz character in the wake.

The data which indicate vortex convection velocities of 60% of the freestream value are in excellent agreement with the wave speed calculation and have enabled velocity vectors to be drawn in a system of coordinates with the vortex street (i.e., in the Lagrangian frame). Two examples are shown in Figs. 15a and 15b. These flowfields, constructed with a phase-angle change of 180 deg, show more clearly the vortex structure and movement. There is obviously some distortion of the flowfield in this simple conversion to the Lagrangian frame since all vortices and turbulence scales do not move at the same velocity. However, the ratio between the lateral and longitudinal vortex spacing of approximately 0.25 compares exceedingly well with the von Karman value of 0.281.[6]

Another feature apparent in both the Eulerian and Lagrangian frames is the dominance of the vertical velocity component in the near-wake. This indicates rapid mixing of the fluid from either side across the vortex street and the previously observed rapid decay in the wake defect. The maximum vortex-induced constant phase-averaged vertical velocities which were observed on the centerline (see, e.g., Fig. 11a) are shown in Fig. 16. It is apparent that fluid crosses the wake axis between vortices with a vertical velocity

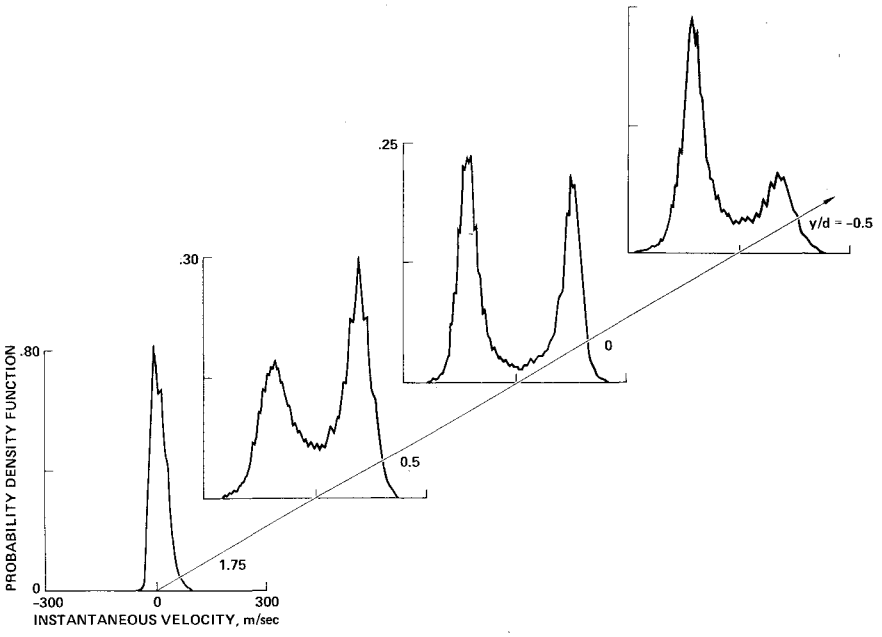

Fig. 11 Vertical velocity probability density.

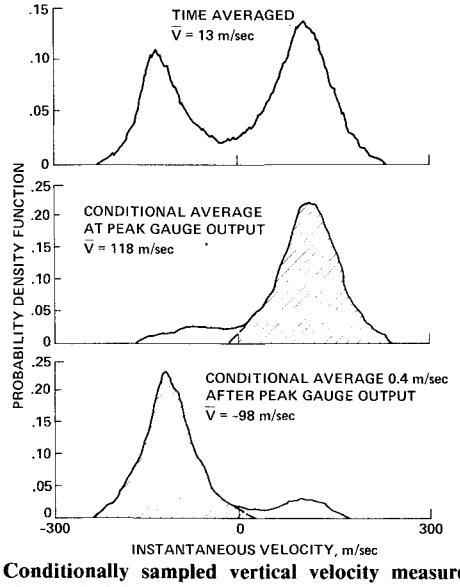

Fig. 12 Conditionally sampled vertical velocity measurements in cylinder wake; $x/d = 2.0$, $y/d = -0.25$.

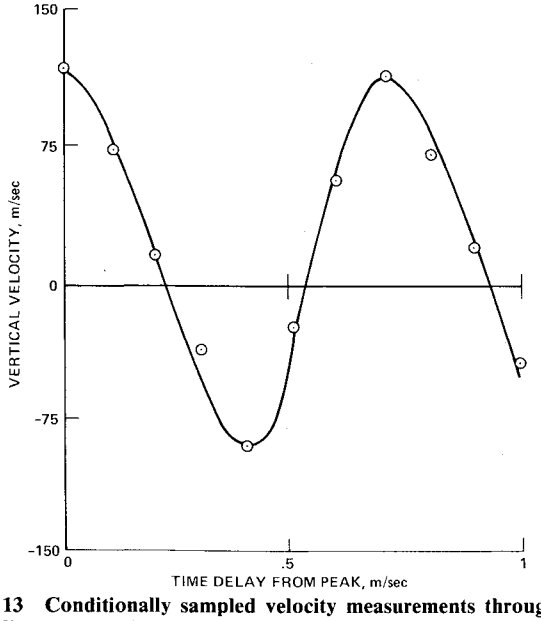

Fig. 13 Conditionally sampled velocity measurements through the shedding cycle; $x/d = 2.0$, $y/d = -0.25$.

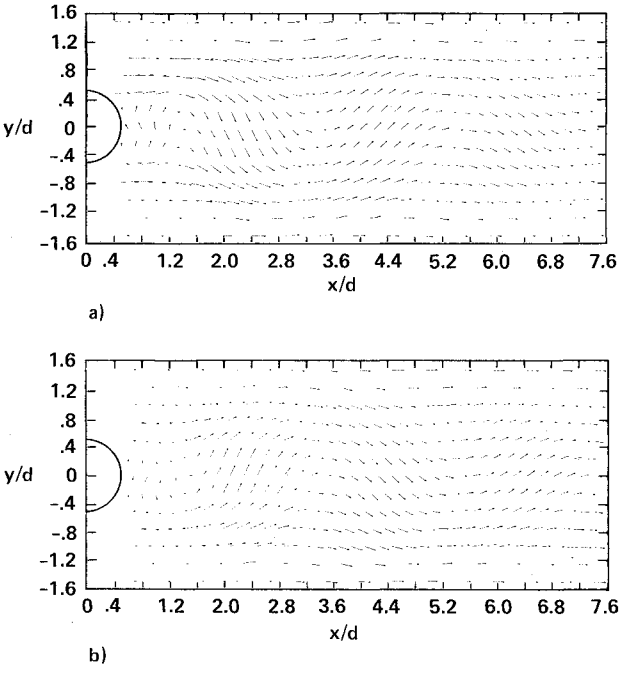

Fig. 14 Cylinder vortex—Eulerian frame; a) phase angle 0 deg, b) phase angle 180 deg.

component in some cases equal to the freestream value. Another interesting feature of the constant phase-averaged vertical velocities is their apparent similarity, when normalized by their maximum-induced value, in the near-wake. Again, these data shown in Fig. 17 are compared with Schlichting's far-wake correlation, and the agreement is extremely good when normalized by the local cross-stream location of zero vertical velocity (y_{max}) and the maximum constant phase-induced velocity.

Turbulence Measurements

We have seen how the periodic character of the processes of vortex formation and convection downstream makes it possible to identify the large-scale structures and to trace their history downstream. Similar techniques can also be used to determine details of the overall and time-dependent turbulent structure of the wake and to obtain insight into the separate small- and large-scale components by conditionally sampling

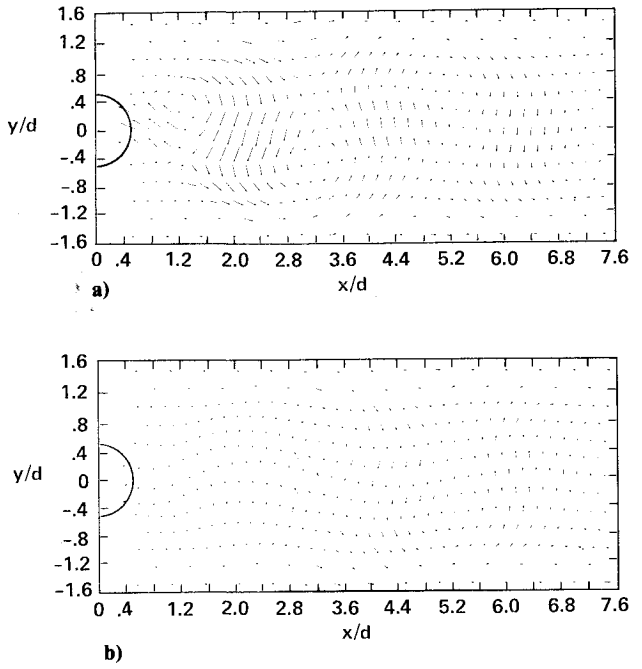

Fig. 15 Cylinder vortex—Lagrangian frame; a) phase angle 0 deg, b) phase angle 180 deg.

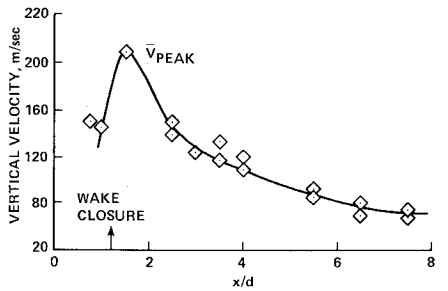

Fig. 16 Mean and rms vertical velocity distribution along the wake centerline.

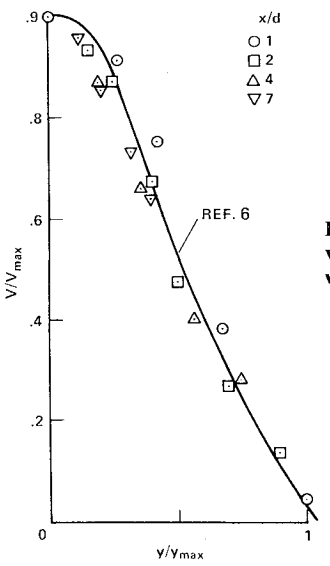

Fig. 17 Nondimensional vertical velocity profiles in the cylinder wake.

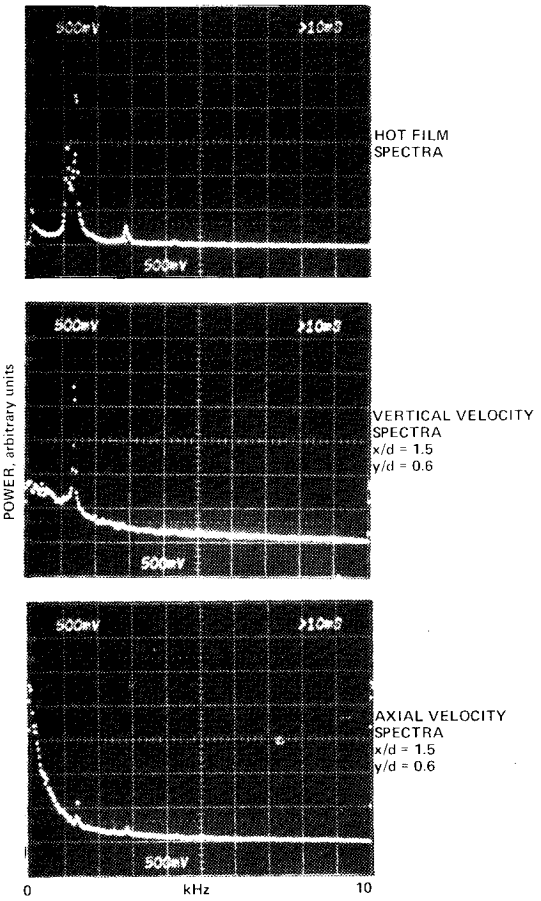

Fig. 18 Hot film and laser anemometer spectra.

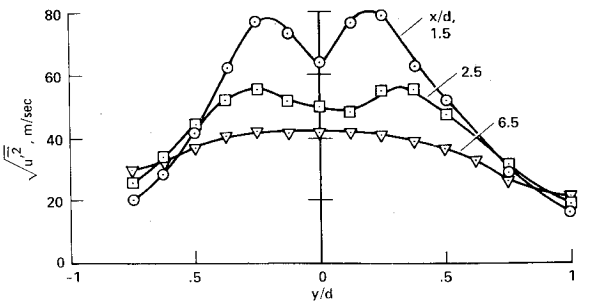

Fig. 19 rms axial velocity profiles.

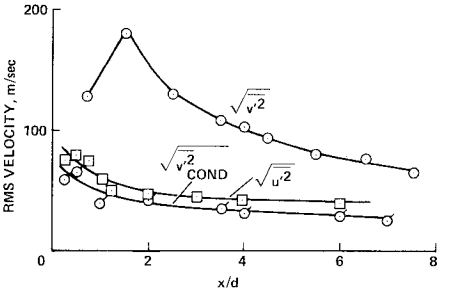

Fig. 20 Axial and conditionally sampled vertical velocity fluctuation levels along the wake.

the velocity data. But, first we should identify the two primary sources of the total turbulent field, namely: the conventional small-scale random velocity fluctuations ($u'_{i,j}$) and the time-dependent (phase-varying) contribution ($\tilde{u}_{i,j}$). As mentioned previously, there is a third source, namely, vortex dispersion, which for simplicity may be apportioned according to scale into $u'_{i,j}$ and $\tilde{u}_{i,j}$. Thus, at any point in the flowfield, we may express the instantaneous velocity (U) as a function of the conventional time average ($\bar{U}$) ,u', and $\tilde{u}$ as

$$U = \bar{U}_{i,j} + u'_{i,j} + \tilde{u}_{i,j}$$

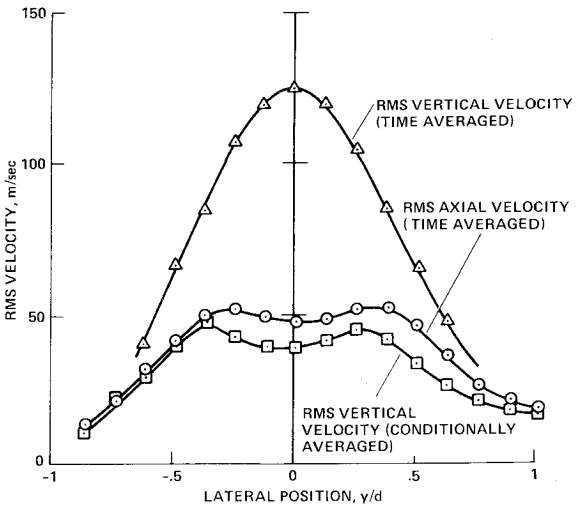

Fig. 21 Time and conditional-averaged turbulent intensities measured in the cylinder wake.

assuming that the small-scale fluctuations and phase-varying velocities are uncorrelated ($\overline{u'_{i,j}\tilde{u}_{i,j}}=0$). Then, we may express the total turbulent velocity fluctuation as

$$U^2_{i,j}-\tilde{U}^2_{i,j}=\overline{u'^2_{i,j}}+\overline{\tilde{u}^2_{i,j}}$$

that is, as the sum of the small-scale and vortex-induced velocity fluctuation levels. The contribution of these two scales can be clearly seen in the spectra of both the surface hot film and laser vertical velocity outputs shown in Fig. 18, where the vortex shedding is characterized by the spike in both spectra at approximately 1400 Hz. Examples of the axial velocity fluctuation levels across the wake are shown in Fig. 19. These data show a series of double peaks located on either side of the wake centerline at the same approximate locations as the vortex centers. This is primarily a result of the fact that fluid velocity on the wake centerline side of each vortex is retarded from the freestream value while fluid on the freestream side is accelerated above the freestream value. Indeed, this large-scale source was also readily apparent in the periodic nature of the axial velocity fluctuations in the near-wake (see Fig. 18). However, due principally to vortex dispersion, these peaks decay quite rapidly downstream.

As previously mentioned, the vertical velocity fluctuation levels are extremely large on the wake centerline. A quantitative picture is given in Fig. 16, where it can be seen that both mean and rms vertical velocities peak in the region of time-averaged wake closure. However (Fig. 20), when phase-sampled, the small-scale turbulence data fall below the axial centerline turbulence measurements. Assuming isotropic small-scale turbulence in the wake, we can infer that there is a vortex-induced contribution to the axial turbulence on the wake centerline. For example, Fig. 21 shows a comparison of the axial and vertical rms velocity fluctuation levels measured across the wake at $x/d=2.5$. As mentioned previously, the apparent vertical velocity fluctuations are extremely high in the center of the wake. However, the conditionally sampled levels are again lower than the axial fluctuation levels, thus indicating a large-scale contribution to the axial turbulence across the entire wake. The large differences in the rms vertical velocity data also show the dominance of the large-scale structures in the vertical wake turbulence. It is clearly incorrect to attempt to model these large rms fluctuation levels with techniques that are only valid for small-scale turbulence. In general, it is equally insufficient to attempt to use current turbulence models scaled to match rms velocities measured in the conventional manner in any flow where unsteady phenomena are likely to be encountered, separated flows being a prime example.

Conclusion

In conclusion, a new and previously unpublished technique which can be used to determine the structure of unsteady turbulent flows has been presented and data obtained in a cylinder wake have been discussed. These data show the time-averaged structure and the detailed time-dependent nature of the wake in both the Eulerian and Lagrangian frames. These conditionally sampled measurements provide information on the vortex positions and spacing. In addition, turbulence data obtained by conventional and conditional averaging of the velocity fluctuations have been presented. These data provide initial measurements of the small- and large-scale contributions to the total turbulent field.

Acknowledgments

This work was supported in part by the Air Force Armament Laboratory, Eglin AFB, Florida, and in part by NASA Ames Research Center, Moffett Field, California, under Contract No. NAS2-9168.

References

[1] Sparks, G. W. and Ezekiel, S., "Laser Streak Velocimetry for Two-Dimensional Flows in Gases," *AIAA Journal*, Vol. 15, March 1977, pp. 110-113.

[2] Davies, M. E., "A Comparison of the Wake Structure of a Stationary and Oscillating Bluff Body Using a Conditional Averaging Technique," *Journal of Fluid Mechanics*, Vol. 75, Pt. 2, 1976, pp. 209-231.

[3] Cantwell, B. J., "A Flying Hot-Wire Study of the Turbulent Wake of a Circular Cylinder at a Reynolds Number of 140,000," Ph.D. Thesis, California Institute of Technology, 1976.

[4] Owen, F. K., "Transition Experiments on a Flat Plate at Subsonic and Supersonic Speeds," *AIAA Journal*, Vol. 8, March 1970, pp. 518-523.

[5] Abramovich, G. N., *The Theory of Turbulent Jets*, The MIT Press, Cambridge, Mass., 1963, pp. 132-133.

[6] Schlichting, H., *Boundary Layer Theory*, 4th ed., McGraw Hill, New York, 1960, p. 602.